

LONG-RANGE SIGNAL TRANSMISSION IN AUTOCRINE RELAYS

Michal Přibyl¹, Cyrill B. Muratov², and Stanislav Y. Shvartsman¹

¹Department of Chemical Engineering and Lewis-Sigler Institute for Integrative Genomics, Princeton University

²Department of Mathematical Sciences and Center for Applied Mathematics and Statistics, New Jersey Institute of Technology

Corresponding Author:

Stanislav Y. Shvartsman

Department of Chemical Engineering and Lewis-Sigler Institute for Integrative Genomics, Princeton University

Tel: 609-258-4694; Fax: 609-258-0211

Princeton, NJ 08544, stas@princeton.edu

Keywords: growth factors, ligand release, intercellular signaling, traveling wave

Running title: Signal transmission in autocrine relays

Abstract

Intracellular signaling induced by peptide growth factors can stimulate release of these molecules. In autocrine and paracrine networks, this can establish a positive feedback loop between ligand binding and ligand release. When coupled to intercellular communication by autocrine ligands, this positive feedback can generate constant-speed traveling waves. To demonstrate that, we propose a mechanistic model of autocrine relay systems. The model is relevant to the physiology of epithelial layers and to a number of in-vitro experimental formats. Using asymptotic and numerical tools, we find that traveling waves in autocrine relays exist and have a number of unusual properties, such as an optimal ligand binding strength necessary for the maximal speed of propagation. We compare our results to recent observations of autocrine and paracrine systems and discuss the steps towards experimental tests of our predictions.

Introduction

The versatility of cell-cell communication relies on sophisticated modules for signal generation, transmission, detection, and processing (Hunter, 2000; Jordan et al., 2000). Compared to signal detection and intracellular transduction, signal generation and transmission are relatively poorly understood. For instance, even though the Epidermal Growth Factor Receptor (EGFR) signaling network has been studied over the past four decades, the molecules that mediate the release of EGFR ligands are being identified only now (Schlessinger, 2000; Lee et al., 2001; Merlos-Suarez et al., 2001; Sunnarborg et al., 2002; Yan et al., 2002). Current work on regulated ligand release focuses on the identification of the relevant molecules and intracellular events (Dello and Rovida, 2002). At the same time, it is important to understand how these processes operate in tissues (Peschon, Slack et al. 1998; Kheradmand and Werb 2002). Here, we suggest a role for regulated ligand release in cell communication within epithelial layers. Motivated by a number of recent reports of nonlinear behavior mediated by autocrine loops (Wasserman and Freeman, 1998; Peri et al., 1999; Mandell et al., 2001; Shvartsman et al., 2002), we develop and analyze a model of ligand generation and transport in autocrine systems. Based on our analysis, we propose a mechanism for a long-range signal transmission in epithelial layers.

Many growth factors and cytokines are released by intracellular or cell surface proteases (Dello and Rovida, 2002). In a number of developmental and physiological contexts, receptor activation is regulated by ligand release and delivery (Freeman and Gurdon, 2002; Kheradmand and Werb, 2002). The availability and activity of ligand-releasing enzymes can be regulated both intra- and extracellularly. Notably, these enzymes can be activated by the signaling pathways that are stimulated by the ligands they release. Therefore, a positive feedback loop can be established in the regime when the producing cell effectively recaptures and responds to the secreted ligand (Carpenter, 1999; Gschwind et al., 2001; Dello and Rovida, 2002). Such feedback from ligand binding to ligand release is a frequent component of autocrine and paracrine EGFR networks (Dent

et al., 1999; Fan and Derynck, 1999; Gechtman et al., 1999; Freeman, 2000; Chen et al., 2001).

Intracellular signaling by the Ras-MAPK pathway can mediate positive feedback in the EGFR system, Figure 1. In *Drosophila*, MAPK activated by EGFR induces the transcription of Rhomboid, an intracellular protease, that processes Spitz, a secreted EGFR ligand (Mantrova and Hsu, 1998; Sapir et al., 1998; Wasserman and Freeman, 1998; Guichard et al., 1999; Bang and Kintner, 2000; Hsu et al., 2001; Lee et al., 2001), Figure 1A. In mammalian EGFR systems, MAPK can activate the cell-surface ligand-releasing proteases, such as TACE and Kuzbanian (Peschon et al., 1998; Fan and Derynck, 1999; Doedens and Black, 2000; Montero et al., 2000; Zhang et al., 2000; Chen et al., 2001; Merlos-Suarez et al., 2001; Umata et al., 2001; Diaz-Rodriguez et al., 2002; Montero et al., 2002; Sunnarborg et al., 2002; Yan et al., 2002), Figure 1B. The MAPK-mediated feedback in the EGFR system is important in a number of developmental and clinical contexts. The EGFR/MAPK/Rhomboid/Spitz feedback functions throughout the fruit fly development (Casci and Freeman, 1999). The EGFR/MAPK/TACE/TGF α network can protect cells against ionizing radiation and prevent the success of cancer radiotherapy (Hagan et al., 2000; Huang and Harari, 2000; Harari and Huang, 2001). These feedbacks rely on the regulation of production and/or activity of ligand-releasing enzymes; other mechanisms relying on the induction of receptor or its ligands have also been described (Doraiswamy et al., 2000; Albanell et al., 2001).

Here, we report a model-based analysis of cell communication in epithelial layers equipped with autocrine positive feedback loops. Our main interest is the mechanisms of signal transmission in autocrine systems. Consider a two-dimensional layer of cells covered by a medium where a soluble ligand can diffuse, Figure 1C. The upper boundary of the medium is impermeable to the ligand. The lower boundary, formed by the cellular layer, can reversibly bind the secreted ligand. The ligand-receptor complexes on the cell surfaces stimulate the intracellular processes leading to further ligand release, Figure 1D. Imagine a quiescent epithelial layer, in which ligand release is in the “off” state, Figure 1C. A localized stimulation of the cellular layer creates a localized source of ligand. As a

result, receptor occupancy and, potentially, ligand release would increase in the neighboring cells. Will this excitation spread across the layer? If yes, then how is the speed of signal transmission in such an “autocrine relay” related to the parameters in the modules for ligand release, binding, transport, and signaling? A mechanistic model of ligand release and transport can provide a systematic framework for addressing these questions. Quantitative measurements of EGFR binding and signaling enable the estimation of the relevant time and length scales (Wiley et al., 1991; Lauffenburger and Linderman, 1993; Dong, 1999; Haugh et al., 1999; Haugh et al., 2000; Burke et al., 2001; DeWitt et al., 2001; Wiley and Burke, 2001). Theory and computations can probe the effects of remaining parameters in the model.

A few words on the considered geometry of cell communication. In vitro, this geometry can be realized within the cell and tissue culture assays, where an epithelial layer or a confluent monolayer of autocrine cells is covered by liquid medium; the experimentalist controls the height of the medium (Mandell et al., 2001). This arrangement is also realized in a number of developmental contexts. For example, in *Drosophila* egg development, a layer of epithelial follicle cells covers a large oocyte (Spradling, 1993; Dobens and Raftery, 2000). Both the oocyte and the follicle cells secrete the EGFR ligands, but EGFR is expressed only in the follicle cells. Hence, ligand diffuses in the gap between the reflective and the receptor-covered surfaces; the size of this gap is less than one micron.

The paper is organized as follows. In the next section we present a model for ligand release, transport, and signaling. We analyze the model using a combination of analytical and computational tools. First, asymptotic techniques are used to solve the simplified version of the model in the regime when receptors are in excess and ligand release obeys a simple threshold-like kinetics. These assumptions are relaxed during the computational analysis of the model. We conclude with the outline of future directions for modeling and suggest experimental tests of our predictions.

Model Formulation

Equations and scaling

We consider an infinite layer of cells covered by an extracellular medium of height h . The model describes the coupled dynamics of secreted ligands (S), surface receptors (R), ligand-receptor complexes (C), and ligand-releasing proteases (P). Let us define the ligand concentration at the cellular layer as $\bar{S}(x, t) \equiv S(x, 0, t)$. Q_R is the rate of receptor synthesis; g_p and g_r denote the linear gains in the protease and ligand production, respectively. The balance equations and the corresponding boundary conditions take the following form:

$$\frac{\partial S}{\partial t} = D \left(\frac{\partial^2 S}{\partial x^2} + \frac{\partial^2 S}{\partial y^2} \right), \quad (1)$$

$$\frac{\partial R}{\partial t} = -k_{on} R \bar{S} + k_{off} C - k_{er} R + Q_r, \quad (2)$$

$$\frac{\partial C}{\partial t} = k_{on} R \bar{S} - (k_{off} + k_{ec}) C, \quad (3)$$

$$\frac{\partial P}{\partial t} = -k_p P + g_p \sigma(C), \quad (4)$$

$$\left(D \frac{\partial S}{\partial y} - k_{on} R S \right) \Big|_{y=0} = -k_{off} C - g_r P \quad \frac{\partial S}{\partial y} \Big|_{y=h} = 0, \quad (5)$$

where t is time, x is the spatial coordinate parallel to the cellular layer, and y is spatial coordinate perpendicular to it (see Figure 1C). The ligand reversibly binds to receptors at the cell surface ($y = 0$). The parameters of the model and their typical values are listed in Table 1.

The production of the ligand-releasing protease, $\sigma(C)$, is described by the sigmoidal function of the number of occupied receptors. This sigmoidal dependence can arise from

the true cooperativity in ligand release and/or from the composition of the intermediate steps between ligand/receptor binding and protease activation.

The model is rendered dimensionless by the following transformations:

$$\tau \equiv tk_p, \quad \zeta \equiv x/L_x, \quad \eta \equiv y/h, \quad s \equiv S/S_0, \quad c \equiv C/C_0, \quad p \equiv P/P_0, \quad r \equiv R/R_0 \quad (6)$$

where

$$\begin{aligned} S_0 &= (k_{off} + k_{ec})(g_r g_p k_{er}) / (k_p k_{on} k_{ec} Q_r), \quad C_0 = (g_r g_p) / (k_p k_{ec}), \\ P_0 &= g_p / k_p, \quad R_0 = Q_r / k_{er}, \quad L_x = (Dk_{er}) / (k_{on} Q_r) \end{aligned} \quad (7)$$

The time scale is set by the dynamics of protease degradation. The vertical length scale is scaled by the height of the medium. The horizontal length scale is derived from the previous analysis of the spatial extent of autocrine loops. Specifically, the length scale L_x appears in the expressions for the cumulative distribution functions that characterize the extrema of random trajectories followed by ligands diffusing above the receptor-covered plane (Shvartsman et al., 2001).

After rescaling, we get:

$$\tau_s \frac{\partial s}{\partial \tau} = \frac{\partial^2 s}{\partial \zeta^2} + \frac{1}{\alpha^2} \frac{\partial^2 s}{\partial \eta^2}, \quad (8)$$

$$\tau_r \frac{\partial r}{\partial \tau} = -\gamma(r\bar{s} - (1-\beta)c) - r + 1 \quad (9)$$

$$\tau_c \frac{\partial c}{\partial \tau} = r\bar{s} - c, \quad (10)$$

$$\frac{\partial p}{\partial \tau} = -p + \sigma(c), \quad (11)$$

$$\left(\frac{\partial s}{\partial \eta} - \alpha r s \right) \Big|_{\eta=0} = -\alpha((1-\beta)c + \beta p) \quad \frac{\partial s}{\partial \eta} \Big|_{\eta=1} = 0. \quad (12)$$

There are six dimensionless parameters in the rescaled model:

$$\begin{aligned} \alpha &= k_{on} R_0 h / D & \beta &= k_{ec} / (k_{off} + k_{ec}) & \gamma &= g_r g_p / (k_p Q_r \beta) \\ \tau_s &= k_p D / (k_{on} R_0)^2 & \tau_c &= k_p / (k_{off} + k_{ec}) & \tau_r &= k_p / k_{er} \end{aligned} \quad (13)$$

The first of these, α , is the Damköhler number that characterizes the relative rates of diffusion and binding (Deen, 1998). Note that α is also the ratio of the geometric and dynamic length scales, h and L_x , respectively. The second dimensionless group, β , characterizes the relative rates of endocytosis and dissociation; γ is proportional to the ratio of the ligand and receptor generation rates (i.e. ratio of $g_r g_p / k_p$ and Q_r); τ_s , τ_r and τ_c characterize the relative time scales of the extracellular ligand, and of the free and bound receptors, respectively.

Steady-state multiplicity and traveling fronts

The spatially uniform steady states of Equations 8-12 satisfy:

$$c - \sigma(c) = 0, \quad r = 1 - \beta\gamma c, \quad p = \sigma(c), \quad s = c / (1 - \beta\gamma c). \quad (14)$$

The first equation is the balance of linear and sigmoidal functions, a classical mechanism for the generation of steady state multiplicity, Figure 2A (Keener, 1998; Fall et al., 2002). Thus, depending on the parameters of the sigmoidal nonlinearity, the system of Equations 14 may have either one or two stable steady states. In the case of bistability, the first of the steady states corresponds to the “off” state of the autocrine loop, with the zero rate of ligand release – $c = 0$, $p = 0$, $r = 1$, $s = 0$. The second steady state corresponds to the

“on” state of the autocrine loop, with nonzero level of ligand-receptor complexes and appreciable rate of ligand release.

We study how the system switches between the two stable steady states of the autocrine loop. In particular, we look for solutions in the form of constant speed traveling fronts that connect these steady states. We analyze the dependence of the front properties on the molecular, cellular, and geometric parameters of the autocrine relays.

Our main finding is that such fronts may indeed be realized in autocrine relay systems. They arise as a result of the coupling of cells by secreted autocrine ligands; this coupling is provided through the diffusion of the ligand in the extracellular space. Note that this form of coupling is different from the one that is usually encountered in models of bistable media, in which an autocatalytic substance both propagates by diffusion and undergoes the autocatalytic reaction at the same time (Mikhailov, 1994; Keener, 1998). In our model, the diffusing variable is just a messenger mediating communication within the layer of autocrine cells. The positive feedback results from the interaction between the messenger and the localized species - in our case, bound receptors and ligand-releasing proteases. Furthermore, the nature of transport in our problem makes the coupling nonlocal. A localized change in the values of non-diffusing variables affects the entire distribution of the messenger concentration. See (Kerner and Osipov, 1994) for examples of such coupling in a number of physical settings.

The fronts are analyzed using a combination of analytical and computational approaches. In the computational experiments, we were starting with the autocrine layer in the “off” state and following the spatiotemporal evolution of the localized disturbance that activated the protease dynamics. We characterize the shape and speed of the traveling front that is established after the initial transient period. In the following, the description of computational experiments is preceded by the discussion of the analytical solution for the fronts in a certain limiting regime. Specifically, we consider the regime that is characterized by the fast dynamics of ligand-receptor complexes, the vast excess of empty receptors, and infinitely sharp nonlinearity of the protease production term. The

analytical solution obtained in this regime enables a complete parametric analysis of the fronts and reveals a number of their unusual properties.

Analytical solution of the simplified model

The ligand-limited regime is characterized by the small ratio of the rates of ligand release and receptor synthesis, $\gamma \ll 1$. In this case, the first term in the right-hand side of the equation 9 for the dynamics of empty receptors can be neglected. As a result, the balance for empty receptors is effectively uncoupled from other variables and the dimensionless concentration of free receptors is constant: $r \approx 1$. When the relaxation of ligand-receptor complexes in the surface layer ($\eta = 0$) is fast, $\tau_c \ll 1$, these species can be eliminated using a pseudo-steady state approximation: $c(\zeta, \tau) = s(\zeta, 0, \tau)$. Thus, under the conditions $\tau_c \ll 1$, $\gamma \ll 1$, the system 8-12 is reduced to the two equations for the extracellular ligand (s), Equation 8, and the ligand-releasing protease (p), Equation A1 in the Appendix. The only source of nonlinearity is provided the sigmoidal generation term in protease dynamics. A sharp sigmoidal nonlinearity can be approximated by a Heaviside function: $\sigma(c) \approx H(c - c_0)$, Figure 2B. In this case, the problem can be solved analytically; see Appendix. The main result is the implicit equation that links the front speed to the geometric, molecular, and cellular parameters of the autocrine loop, Equation A18. This equation was solved graphically to produce the parametric plots in the next section.

Results and Discussion

Fronts in the asymptotic regime

In the ligand-limited regime ($\gamma \ll 1$) with fast binding ($\tau_c \ll 1$) and sharp nonlinearity ($\sigma(c) \approx H(c - c_0)$), the properties of propagating fronts depend on four dimensionless parameters. The value of c_0 defines the threshold of the nonlinearity, τ_s is the relative time scale for the relaxation of the extracellular ligand, α compares the rates of binding

and transport, β depends on the kinetic parameters of the ligand-receptor complex. Given the values of these parameters, the formulas derived in the Appendix provide the spatial profile and the speed of the propagating front. Figure 3 presents the spatial profiles of ligand and protease for a particular set of parameters corresponding to advancing “on” state of the autocrine loop.

The molecular and cellular parameters, such as the density of cell surface receptors ($R_0 = Q_r / k_{er}$) and binding rate constant (k_{on}) appear in several dimensionless groups; hence, their effect on the front properties is not immediately obvious. In the ligand-limited regime, the total number of receptors and the rate constant of the forward binding reaction always appear as a product, $k_{on}R_0$, that characterizes the intensity of ligand binding; this product has the dimension of velocity. The kinetic properties of the ligand-receptor complex are combined in the dimensionless ratio of rates of dissociation and internalization: $k_{ec} / (k_{off} + k_{ec})$. The geometric length scale, h , appears in the Damköhler number, α , that regulates the nonuniformity of solution in the vertical direction, see Equations 8, 12.

Figures 4 and 5 show the effects of molecular, cellular, and geometric parameters on the speed of the propagating solutions. We fix the diffusion coefficient and the height of the extracellular medium and analyze the effect of the binding and trafficking parameters. The height of the medium is 1 mm, a typical value encountered in cell and tissue culture assays of autocrine loops (DeWitt et al., 2001); ligand diffusivity is set to $10^{-6} \text{ cm}^2\text{s}^{-1}$, a typical value for the diffusivity of a protein in solution.

Figure 4A presents a two-parameter plot of the front speed on the rate of forward-binding reaction (k_{on} and R_0) and the kinetic properties of ligand-receptor complexes (k_{ec} and k_{off}). Interestingly, we find that the front speed has a maximum with respect to the intensity of forward binding reaction. In particular, for any given value of the kinetic rate constants, there exists an optimal number of cell surface receptors. The speed of the front

is maximal at this optimal value; see Figure 4B for the typical one-dimensional cut through the two-parameter plot in Figure 4A.

The nonmonotonic dependence of the front speed on the number or surface receptors and/or the forward binding rate constant is a result of the particular nature of coupling in autocrine relays. A sufficient number of cell surface receptors must be occupied in order to sustain the protease activation; this explains the ascending part of the curve. At the same time, the traveling front is slowed down when ligand spends most of its time bound to cell surface receptors; this qualitatively explains the descending part of the curve. A more detailed study of the parametric dependences of the velocity will be presented elsewhere. The maximum in the dependence of the front speed on $k_{on}R_0$ is robust property of autocrine relays; it exists for any value of the threshold in the nonlinearity and the rate constants of dissociation and internalization. The speed of the front depends on the kinetic properties of ligand-receptor binding. Hence, it is not possible to compare front speeds in ligand-receptor systems based only on the corresponding equilibrium binding constant.

The height of the medium can be easily adjusted in cell and tissue culture assays. Figure 5A presents the dependence of the front speed on the ratio of the geometric and dynamic length scales in the problem (i.e. ratio of h and L_x). When the ratio of these two length scales is small, the front speed is an increasing function of the medium height. Once again, this is the result of the nature of coupling in autocrine epithelial layers. For small height of the medium, the time interval between successive binding events of secreted ligand is short; the ligand spends a large fraction of its time in the bound form. Consequently, increasing the height of the medium increases both the duration and the span of the ligand trajectories and, as a result, the speed of the propagating front. In this regime, the fronts are essentially one-dimensional, in a sense that they are nearly uniform in the vertical direction; see the two top profiles in Figure 5B. This is easy to understand: the small value of the medium height translates into the low value of the Damköhler number, α , that determines variation of the solution in the vertical direction, see Equations 8-12. In fact, a conventional “thin fin” approximation (Deen 1998) derived in

the limit $\alpha \rightarrow 0$ captures these fronts and their dependence on the height of the medium very accurately (results not shown).

When the height of the medium is comparable to the dynamical length scale L_x of the problem, the fronts become fully two-dimensional; see the two bottom profiles in Figure 5B. The dependence of the front speed on the medium's height h asymptotically approaches a constant value, Figure 5A. This behavior can be explained in terms of the results of a recent analysis of autocrine loops in the semiinfinite medium (Shvartsman et al., 2001). The statistical properties of both the vertical and the lateral spans of the random trajectories followed by autocrine ligands are characterized by the single length scale given by L_x . Specifically, half of the ligand trajectories are captured for the first time before their maximal lateral displacement reaches L_x . This is precisely the dynamical length scale in our problem, see Equation 6. In other words, autocrine loops are spatially localized even in the semiinfinite medium. This means that, above some critical value, increasing the height of the medium would stop contributing to the effective range of the messenger variable in our problem. Consequently, the dependence of the front speed on the height of the medium should vanish at high ratios of the geometric and the dynamic length scales in the problem, Figure 5A.

Numerical Simulations of Propagating Fronts

The analysis of the traveling fronts in the ligand-limited regime with fast binding and sharp nonlinearity of protease activation relies on a number of assumptions about the relative time scales of the processes in autocrine relays. To test the predictions of the asymptotic analysis, we carried out direct numerical simulations of the full model described by Equations 8-12. The spatial derivatives in Equations 8 and 12 were replaced by finite differences and the resulting set of ODEs was solved using the RKC (Sommeijer et al., 1998). Our main result can be summarized as follows: traveling fronts predicted in the simplified model exist for a wide range of parameters in the full model. Moreover, they exhibit the properties predicted by the analysis of the simplified model.

Figures 6A,B present the profile of the fully developed front computed in the full model with the Hill nonlinearity, a nonzero value of the time scale of ligand receptor complex, and a nonnegligible ratio of the ligand and receptor generation rates. This front was computed in a transient simulation that started with the system in the “off state” and followed the evolution of a localized disturbance activating the ligand release. After the initial transient, this disturbance evolves into a fully developed self-similar solution – a constant speed front, Figure 6C. Figure 6D shows that, in agreement with the predictions of the analysis of the ligand-limited regime with fast binding and sharp nonlinearity of protease activation, the speed of the fronts in the full model exhibits a maximum with respect to the intensity of the binding process ($k_{on}R_T$).

Finally, we use numerical simulations of the full model to analyze the interaction of propagating fronts with heterogeneities in the cellular layer. Our computational experiments are motivated by recent observations of Mandell and coworkers (Mandell et al., 2001). They have visualized the spatiotemporal dynamics of ERK2/MAPK activation that was induced in the layer of astroglial cells by a localized injury. Such a stimulus induced a wave-like transient that propagated away from the injured region of the epithelium, Figure 3 in Mandell et al (Mandell et al., 2001). They have suggested that this effect is mediated by a paracrine relay mechanism that is initiated at the place of injury. To support their hypothesis, they have shown that waves induced by the localized mechanical stimulus can “jump over” the gaps in the cellular layer. Hence, signal transmission is not mediated by direct cell-cell contact, but depends on diffusing signal.

Figure 7 illustrates that traveling waves in the model of autocrine relays can “jump” over the heterogeneities in the cellular layer. This behavior is not unexpected, since the mechanism of signal transmission is mediated by diffusion through the extracellular medium. What is interesting, however, is that the fronts can be both accelerated and impeded by the heterogeneities. This effect can be explained by the maximum in the dependence of the front speed on the number of cell surface receptors, Figure 6D. When the parameters of the monolayer correspond to the ascending part of the curve, the front is slowed down by the heterogeneity. In this regime, the heterogeneity provides a

localized break in the positive feedback loop, Figure 7B. However, to the right of the maximum, when the front speed is a decreasing function of the number of receptors, the front will be accelerated by the local heterogeneity. In this regime, the front motion in the unperturbed layer is slowed down by frequent ligand-receptor binding. Thus, heterogeneity characterized by the absence of cell surface receptors provides a localized “escape path” for autocrine ligands, increasing the range of their action, Figure 7C. Notice that in both cases the fronts regain the constant velocity after their interaction with local heterogeneity. This computational experiment underscores the unusual properties of traveling waves in autocrine systems.

Conclusions

We have developed a mechanistic model of autocrine relays. The model enables a systematic analysis of nonlinear interaction between ligand release, transport, and binding. Our transport model accounts for the nonlocal coupling between different regions of the epithelial layer; the range of the coupling is directly related to the transport, binding, and endocytosis of the secreted ligand. When combined with a positive feedback by ligand release, the model robustly predicts the existence of propagating fronts. These fronts travel at constant speeds and can deliver signals to arbitrary distances. This wave-like propagation is very different from the one that relies on pure diffusion. Specifically, we predict the existence of traveling waves mediated by the autocrine release of growth factors. In other systems, traveling waves can be mediated by the regulated release of extracellular calcium, ATP, cAMP (Kessler and Levine, 1993; Tang and Othmer, 1995; Tang et al., 1996; Palsson et al., 1997; D'andrea et al., 1998; Muller et al., 1998; Sneyd et al., 1998; Homolya et al., 2000; Scemes et al., 2000; Dormann et al., 2001; Shiga et al., 2001; Hofer et al., 2002; Schuster et al., 2002). The fronts mediated by autocrine loops have a number of unusual properties, such as a nonmonotonic dependence of the front speed on the total number of surface receptors and/or the forward binding rate constant.

At this point, there is no direct evidence for traveling waves mediated by the regulated secretion of peptide growth factors. Recently, however, a paracrine mechanism has been

proposed to cause the wave-like spread of signaling activity induced by localized mechanical stimulus (Mandell et al., 2001). A wealth of experiments supporting the release-mediated positive feedback in growth factor systems indicates that these waves can be observed (Hunter, 1998; Carpenter, 1999; Dent et al., 1999; Fan and Derynck, 1999; Gechtman et al., 1999; Moghal and Sternberg, 1999; Albanell et al., 2001; Chen et al., 2001; Gschwind et al., 2001; Ma et al., 2001; Merlos-Suarez et al., 2001; Murphy et al., 2001; Carraway and Sweeney, 2002; Diaz-Rodriguez et al., 2002; Montero et al., 2002). Usually, this feedback is studied in cell culture, where cells are randomly dispersed on the surface. We predict that experiments with confluent cell monolayers or with model epithelial layers will uncover traveling waves mediated by autocrine growth factors. The EGFR network is a particularly promising experimental system. The experiments require an ability to locally stimulate ligand release and to follow the progress of activation across the cellular layer. Localized stimulation can be mechanical, chemical, or rely on gamma or UV radiation. Excitation can be followed either in-situ (e.g., using fluorescent reporters) or ex-situ (e.g., using Western blots epithelial layers at different time points). The A431 carcinoma cell line with a positive EGFR/MAPK/TGF α feedback is a good experimental system for these studies (Dent et al., 1999; Shvartsman et al., 2002). Cell surface receptor density can be regulated by addition of antireceptor antibodies (Forsten and Lauffenburger, 1992; Lauffenburger et al., 1995).

Our continuum model allows gradients of localized variables, e.g., the intracellular activity, at the length scale less than a single cell. In order to explore the relevance of our predictions to the in-vivo physiology and development of epithelial layers, it might be necessary to adapt our model in order to explicitly resolve individual cells. In this model localized variables will be considered space-independent inside the cells. These discrete elements will be coupled by diffusion through the extracellular medium. The behavior of this hybrid model is expected to significantly differ from the predictions of the fully continuum model in the regimes where the length scale for ligand transport and the height of the medium become comparable to the size of a single cell. In this regime, we expect the existence of localized patterns.

Almost invariably, nonlinear traveling waves in cell communication are modeled as reaction-diffusion systems, where the amplification processes in the active medium happens in the same region as transport. In our model, these processes are separated in a sense that active processes at different parts of the surface are nonlocally coupled by diffusion through the volume. The properties of traveling waves in such systems are yet to be characterized in details; this work is currently underway in our group.

The positive feedback from ligand binding to ligand release is just one of the many regulatory patterns in autocrine and paracrine networks. Some of the other mechanisms involve binding-stimulated receptor shedding (Ni et al., 2001), decrease of receptor mRNA stability (Sturtevant et al., 1994), and release of extracellular ligand/binding components (Guan et al., 2001; Freeman and Gurdon, 2002; Gerlitz and Basler, 2002). The physiological significance of these processes is only starting to be appreciated. We suggest that a combination of computational and experimental approaches to local growth factor networks may become indispensable for uncovering their role in tissue physiology (Slepchenko et al., 2002).

The next stage of modeling should account for the dynamics of intracellular signaling. A number of “lumped” models of EGFR signaling can be incorporated into our models of autocrine epithelial layers (Bhalla and Iyengar, 1999; Kholodenko et al., 1999; Brighman and Fell, 2000; Haugh et al., 2000; Schoeberl et al., 2002). For this, a model of protease dynamics is necessary. A simplified description, accounting for the stimulation-induced downregulation of the protease and the kinetic patterns of EGFR ligand release, has been recently developed (Dong, 1999; Fan and Derynck, 1999; Gechtman et al., 1999; Doedens and Black, 2000; Shvartsman et al., 2002). A growing number of studies of regulated ligand release can be used to develop and validate a more detailed model. This model would simultaneously account for multiple species and processes leading to binding-induced ligand release (Zhang et al., 2000; Albanell et al., 2001; Merlos-Suarez et al., 2001; Pierce et al., 2001; Umata et al., 2001; Dello and Rovida, 2002; Diaz-Rodriguez et al., 2002; Kheradmand and Werb, 2002; Montero et al., 2002; Sunnarborg

et al., 2002). Once this is accomplished, computational analysis of autocrine relays can be used to study the properties of traveling waves and to guide their experimental analysis.

ACKNOWLEDGMENTS

Our work has been supported by the National Science Foundation.

Appendix

The analytical solution is constructed in the limiting case of $\tau_c \rightarrow 0$, $\gamma \rightarrow 0$, and $\sigma(c) = H(c - c_0)$, where $H(x)$ is the Heaviside function and c_0 is the threshold. Under these assumptions, we have $r = 1$ and $c(\xi, \tau) = \bar{s}(\xi, \tau)$ on the time scale of the wave, so Equations 9-12 simplify to

$$\frac{\partial p}{\partial \tau} = -p + H(\bar{s} - c_0), \quad (\text{A1})$$

$$\left(\frac{\partial s}{\partial \eta} - \alpha \beta s \right) \Big|_{\eta=0} = -\alpha \beta p \quad \frac{\partial s}{\partial \eta} \Big|_{\eta=1} = 0. \quad (\text{A2})$$

We are looking for the traveling wave solutions $s = s(\zeta - v\tau, \eta)$, $p = p(\zeta - v\tau)$ connecting the steady state $s = 1$, $p = 1$ at $\zeta = -\infty$ with the steady state $s = 0$, $p = 0$ at $\zeta = +\infty$, moving with speed $v > 0$ to the right. Introducing the reference frame moving with the wave

$$\xi \equiv \zeta - v\tau, \quad (\text{A3})$$

and rewriting, Equations 8, A1 in terms of ξ , we obtain

$$\frac{\partial^2 s}{\partial \xi^2} + v\tau_s \frac{\partial s}{\partial \xi} + \frac{1}{\alpha^2} \frac{\partial^2 s}{\partial \eta^2} = 0 \quad (\text{A4})$$

$$v \frac{\partial p}{\partial \xi} - p + H(-\xi) = 0, \quad s(0, 0) = c_0, \quad (\text{A5})$$

where we assumed that $s(\xi, 0)$ is a monotonically decreasing function of ξ and placed the point of the onset of the protease production at the origin.

Equation A5 can be straightforwardly integrated

$$p(\xi) = H(-\xi)(1 - \exp(\xi/v)) \quad (\text{A6})$$

This solution can be substituted into Equations A2, A4, which can then be solved by separation of variables. Let us look for the solution of Equations A2, A4 in the form

$$s(\xi, \eta) = p(\xi) + \sum_{n=1}^{\infty} \phi_n(\xi) \psi_n(\eta), \quad (\text{A7})$$

where $\psi_n(\eta)$ are the orthonormal eigenfunctions of the Sturm-Liouville problem

$$\psi_n'' + \lambda_n^2 \psi_n = 0, \quad \psi_n'(0) - \alpha\beta \psi_n(0) = 0, \quad \psi_n'(1) = 0. \quad (\text{A8})$$

A simple calculation gives

$$\lambda_n \tan(\lambda_n) = \alpha\beta \quad n = 1, 2, 3, \dots, +\infty \quad (\text{A9})$$

$$\psi_n(\eta) = \left[2\lambda_n / [\lambda_n + \sin \lambda_n \cos \lambda_n] \right]^{\frac{1}{2}} \cos(\lambda_n - \lambda_n \eta). \quad (\text{A10})$$

Substituting Equation A7 into A4, multiplying it by ψ_n , and then integrating over η , we obtain an equation for $\phi_n^\pm(\xi)$, where $\phi_n^+(\xi)$ and $\phi_n^-(\xi)$ are the solutions for $\xi > 0$ and $\xi < 0$, respectively:

$$\frac{d^2 \phi_n^\pm}{d\xi^2} + v\tau_s \frac{d\phi_n^\pm}{d\xi} - \frac{\lambda_n^2}{\alpha^2} \phi_n^\pm = \left[\frac{2}{\lambda_n (\lambda_n + \sin \lambda_n \cos \lambda_n)} \right]^{\frac{1}{2}} \frac{(1 + v^2 \tau_s) \sin \lambda_n \exp(\xi/v) H(-\xi)}{v^2} \quad (\text{A11})$$

This equation has to be supplemented by the boundary conditions at $\xi = 0$ and $\xi \rightarrow \pm\infty$. At infinity we must use the exact fact that $s(+\infty, 0) = 0$ and $s(-\infty, 0) = 1$. We should also use the fact that s together with its first derivatives must be continuous at $\xi = 0$. In view of Equation A7, this translates to

$$\sum_{n=1}^{\infty} \phi_n^+(0) \psi_n(\eta) = \sum_{n=1}^{\infty} \phi_n^-(0) \psi_n(\eta), \quad (\text{A12})$$

$$\sum_{n=1}^{\infty} \psi_n(\eta) \left. \frac{d\phi_n^+}{d\xi} \right|_{\xi=0} = \sum_{n=1}^{\infty} \psi_n(\eta) \left. \frac{d\phi_n^-}{d\xi} \right|_{\xi=0} - v^{-1}. \quad (\text{A13})$$

Once again, multiplying Equations A12, A13 by ψ_n , integrating over η and combining them with the behavior at infinity, we obtain that ϕ_n^\pm should satisfy the following boundary equation

$$\phi_n^\pm(\pm\infty) = 0, \quad \phi_n^+(0) = \phi_n^-(0) \quad (\text{A14})$$

$$\left. \frac{d\phi_n^+}{d\xi} \right|_{\xi=0} = \left. \frac{d\phi_n^-}{d\xi} \right|_{\xi=0} - \left[\frac{2}{\lambda_n (\lambda_n + \sin \lambda_n \cos \lambda_n)} \right]^{\frac{1}{2}} \frac{\sin \lambda_n}{v}. \quad (\text{A15})$$

After a rather long, but straightforward calculation, we obtain

$$\phi_n^+(\xi) = \frac{\alpha \sin \lambda_n \exp \left\{ - \left[v \alpha \tau_s + (4\lambda_n^2 + v^2 \alpha^2 \tau_s^2)^{\frac{1}{2}} \right] \xi / (2\alpha) \right\}}{\left[2\lambda_n (\lambda_n + \sin \lambda_n \cos \lambda_n) \right]^{\frac{1}{2}}} \times \frac{v \left[\tau_s \alpha^2 (\tau_s v^2 + 1) + 2\lambda_n^2 \right] - \alpha (\tau_s v^2 + 1) (4\lambda_n^2 + v^2 \alpha^2 \tau_s^2)^{\frac{1}{2}}}{\left[v^2 \lambda_n^2 - \alpha^2 (\tau_s v^2 + 1) \right] (4\lambda_n^2 + v^2 \alpha^2 \tau_s^2)^{\frac{1}{2}}}, \quad (\text{A16})$$

and

$$\begin{aligned}
\phi_n^-(\xi) = & \frac{\alpha \sin \lambda_n \exp \left\{ - \left[v \alpha \tau_s - (4\lambda_n^2 + v^2 \alpha^2 \tau_s^2)^{\frac{1}{2}} \right] \xi / (2\alpha) \right\}}{\left[2\lambda_n (\lambda_n + \sin \lambda_n \cos \lambda_n) \right]^{\frac{1}{2}}} \times \\
& \frac{v \left[\tau_s \alpha^2 (\tau_s v^2 + 1) + 2\lambda_n^2 \right] + \alpha (\tau_s v^2 + 1) (4\lambda_n^2 + v^2 \alpha^2 \tau_s^2)^{\frac{1}{2}}}{\left[v^2 \lambda_n^2 - \alpha^2 (\tau_s v^2 + 1) \right] (4\lambda_n^2 + v^2 \alpha^2 \tau_s^2)^{\frac{1}{2}}} \\
& \frac{2\alpha^2 (\tau_s v^2 + 1) \sin \lambda_n \exp(\xi/v)}{\left[v^2 \lambda_n^2 - \alpha^2 (\tau_s v^2 + 1) \right] \left[2\lambda_n (\lambda_n + \sin \lambda_n \cos \lambda_n) \right]^{\frac{1}{2}}}.
\end{aligned} \tag{A17}$$

Substituting this solution into Equation A7 and using it in the self-consistency condition in Equation A5, we obtain the implicit expression for the speed of the traveling wave

$$c_0 = \sum_{n=1}^{\infty} \frac{4\alpha \lambda_n^2 \sin \lambda_n \cos \lambda_n / (\lambda_n + \sin \lambda_n \cos \lambda_n)}{\alpha (\tau_s v^2 + 1) (4\lambda_n^2 + v^2 \alpha^2 \tau_s^2) + v \left[2\lambda_n^2 + \alpha^2 \tau_s (\tau_s v^2 + 1) \right] (4\lambda_n^2 + v^2 \alpha^2 \tau_s^2)^{\frac{1}{2}}} \tag{A18}$$

- Albanell, J., J. Codony-Servat, F. Rojo, J.M. Del Campo, S. Sauleda, J. Anido, G. Raspall, J. Giralit, J. Rosello, R.I. Nicholson, J. Mendelsohn, J. Baselga. 2001. Activated extracellular signal-regulated kinases: association with epidermal growth factor receptor/ transforming growth factor α expression in head and neck squamous carcinoma and inhibition by anti-epidermal growth factor treatments. *Cancer Res* 61:6500-6510.
- Bang, A.G., C. Kintner. 2000. Rhomboid and Star facilitate presentation and processing of the Drosophila TGF- α homolog Spitz. *Genes and development* 14:177-186.
- Bhalla, U., R. Iyengar. 1999. Emergent properties of networks of biological signaling pathways. *Science* 283:339-40.
- Brighthman, F.A., D.A. Fell. 2000. Differential feedback regulation of the MAPK cascade underlies the quantitative differences in EGF and NGF signaling in PC12 cells. *FEBS Letters* 482:169-74.
- Burke, P., K. Schooler, H.S. Wiley. 2001. Regulation of epidermal growth factor receptor signaling by endocytosis and intracellular trafficking. *Mol Cell Biol* 21:1897-910.
- Carpenter, G. 1999. Employment of the epidermal growth factor receptor in growth factor-independent signaling pathways. *Journal of Cell Biology* 146:697-702.
- Carraway, K.L., C. Sweeney. 2002. EGF receptor activation by heterologous mechanisms. *Cancer Cell* 1:405-6.
- Casci, T., M. Freeman. 1999. Control of EGF receptor signalling: Lessons from fruitflies. *Cancer And Metastasis Reviews* 18:181-201.
- Chen, N., W.Y. Ma, Q.B. She, E. Wu, G. Liu, A.M. Bode, Z. Dong. 2001. Transactivation of the epidermal growth factor receptor is involved in 12-O-tetradecanoylphorbol-13-acetate-induced signal transduction. *J Biol Chem* 276:46722-8.
- D'andrea, P., A. Calabrese, M. Grandolfo. 1998. Intercellular calcium signalling between chondrocytes and synovial cells in co-culture. *Biochem. J*, 329:681-7.
- Deen, W.M. 1998. Analysis of transport phenomena. Oxford University Press, New York
- Dello, S., E. Rovida. 2002. Transmodulation of cell surface regulatory molecules via ectodomain shedding. *Biol Chem* 383:69-83.
- Dent, P., D. Reardon, J. Park, G. Bowers, C. Logsdon, K. Valerie, R. Schmidt-Ullrich. 1999. Radiation-induced release of transforming growth factor α activates the epidermal growth factor receptor and mitogen-activated protein kinase pathway in carcinoma cells, leading to increased proliferation and protection from radiation-induced cell death. *Molecular biology of the cell* 10:2493-2506.
- DeWitt, A., J. Dong, H. Wiley, D. Lauffenburger. 2001. Quantitative analysis of the EGF receptor autocrine system reveals cryptic regulation of cell response by ligand capture. *J Cell Sci* 114:2301-13.
- Diaz-Rodriguez, E., J.C. Montero, A. Esparis-Ogando, L. Yuste, A. Pandiella. 2002. Extracellular Signal-regulated Kinase Phosphorylates Tumor Necrosis Factor α -converting Enzyme at Threonine 735: A Potential Role in Regulated Shedding. *Mol Biol Cell* 13:2031-44.
- Dobens, L.L., L.A. Raftery. 2000. Integration of epithelial patterning and morphogenesis in Drosophila oogenesis. *Developmental dynamics* 218:80-93.

- Doedens, J.R., R.A. Black. 2000. Stimulation-induced down-regulation of tumor necrosis factor- alpha converting enzyme. *Journal Of Biological Chemistry* 275:14598-14607.
- Dong, J.Y., Wiley, H. S. 1999. Trafficking and proteolytic release of epidermal growth factor receptor ligands are modulated by their membrane-anchoring domains. *Journal Of Biological Chemistry* 275:557-564.
- Doraiswamy, V., J. Parrot, M. Skinner. 2000. Expression and action of transforming growth factor alpha in normal ovarian surface epithelium and ovarian cancer. *Biol Reprod* 63:789-96.
- Dormann, D., J. Kim, P. Devreotes, C. Weijer. 2001. cAMP receptor affinity controls wave dynamics, geometry and morphogenesis in Dictyostelium. *J Cell Sci* 114:2513-23.
- Fall, C., E. Marland, E. Wagner, J.J. Tyson, editors. 2002. Computational Cell Biology. New York: Springer.
- Fan, H.Z., R. Derynck. 1999. Ectodomain shedding of TGF-alpha and other transmembrane proteins is induced by receptor tyrosine kinase activation and MAP kinase signaling cascades. *Embo Journal* 18:6962-6972.
- Forsten, K.E., D.A. Lauffenburger. 1992. Interrupting Autocrine Ligand-Receptor Binding - Comparison Between Receptor Blockers and Ligand Decoys. *Biophysical Journal* 63:857-861.
- Freeman, M. 2000. Feedback control of intercellular signalling in development. *Nature* 408:6810.
- Freeman, M., J.B. Gurdon. 2002. Regulatory Principles of Developmental Signaling. *Annu Rev Cell Dev Biol* 18.
- Gechtman, Z., J.L. Alonso, G. Raab, D.E. Ingber, M. Klagsbrun. 1999. The shedding of membrane-anchored heparin-binding epidermal- like growth factor is regulated by the Raf/mitogen-activated protein kinase cascade and by cell adhesion and spreading. *Journal Of Biological Chemistry* 274:28828-28835.
- Gerlitz, O., K. Basler. 2002. Wingful, an extracellular feedback inhibitor of Wingless. *Genes Dev* 16:1055-9.
- Gschwind, A., E. Zwick, N. Prenzel, M. Leserer, A. Ullrich. 2001. Cell communication networks: epidermal growth factor receptor transactivation as the paradigm for interreceptor signal transmission. *Oncogene* 20:1594-1600.
- Guan, R., Y. Zhang, J. Jiang, C. Baumann, R. Black, G. Baumann, S. Frank. 2001. Phorbol Ester- and Growth Factor Induced Growth Hormone (GH) proteolysis and GH-binding protein shedding: relationship to GH receptor downregulation. *Endocrinology* 142:1137-1147.
- Guichard, A., B. Biehs, M.A. Sturtevant, L. Wickline, J. Chacko, K. Howard, B. E. 1999. rhomboid and Star interact synergistically to promote EGFR/MAPK signaling during Drosophila wing vein development. *Development* 126:2663-76.
- Hagan, M., L. Wang, J.R. Hanley, J.S. Park, P. Dent. 2000. Ionizing radiation-induced mitogen-activated protein (MAP) kinase activation in DU145 prostate carcinoma cells: MAP kinase inhibition enhances radiation-induced cell killing and G(2)/M-Phase arrest. *Radiation Research* 153:371-383.

- Harari, M., S. Huang. 2001. Radiation response modification following molecular inhibition of epidermal growth factor receptor signaling. *Semin Radiat Oncol* 11:281-9.
- Haugh, J., A. Huang, H. Wiley, A. Wells, D. Lauffenburger. 1999. Internalized epidermal growth factor receptors participate in the activation of p21(ras) in fibroblasts. *J Biol Chem* 274:34350-60.
- Haugh, J., A. Wells, D. Lauffenburger. 2000. Mathematical modeling of epidermal growth factor receptor signaling through the phospholipase C pathway: mechanistic insights and predictions for molecular interventions. *Biotechnol Bioeng* 70:225-38.
- Hofer, T., L. Venance, C. Giaume. 2002. Control and plasticity of intercellular calcium waves in astrocytes: a modeling approach. *Biophys J* 22:4850-9.
- Homolya, L., T.H. Steinberg, R.C. Boucher. 2000. Cell to cell communication in response to mechanical stress via bilateral release of ATP and UTP in polarized epithelia. *J Cell Biol* 150:1349-60.
- Hsu, T., D. McRackan, T.S. Vincent, H. Gert de Couet. 2001. Drosophila Pin1 prolyl isomerase Dodo is a MAP kinase signal responder during oogenesis. *Nature Cell Biology* 3:538-43.
- Huang, S., P. Harari. 2000. Modulation of radiation response after epidermal growth factor blockade in squamous cell carcinomas: inhibition of damage repair, cell cycle kinetics, and tumor angiogenesis. *Clinical Cancer Research* 6:2166-74.
- Hunter, T. 1998. The Croonian Lecture 1997. The phosphorylation of proteins on tyrosine: its role in cell growth and disease. *Philos Trans R Soc Lond B Biol Sci* 353:583-605.
- Hunter, T. 2000. Signaling - 2000 and beyond. *Cell* 100:113-27.
- Jordan, J., E. Landau, R. Iyengar. 2000. Signaling networks: the origins of cellular multitasking. *Cell* 103:193-200.
- Keener, J. 1998. *Mathematical Physiology*. Springer, New York
- Kerner, B.S., V.V. Osipov. 1994. *Autosolitons*. Kluwer Academic, Dordrecht
- Kessler, D.A., H. Levine. 1993. Pattern formation in Dictyostelium via the dynamics of cooperative biological entities. *Phys Rev E* 48:4801-4804.
- Kheradmand, F., Z. Werb. 2002. Shedding light on sheddases: role in growth and development. *Bioessays* 24:8-12.
- Kholodenko, B.N., O.V. Demin, G. Moehren, J.B. Hoek. 1999. Quantification of short term signaling by the epidermal growth factor receptor. *Journal Of Biological Chemistry* 274:30169-30181.
- Lauffenburger, D.A., K.E. Forsten, B. Will, H.S. Wiley. 1995. Molecular/Cell Engineering Approach to Autocrine Ligand Control of Cell-Function. *Annals Of Biomedical Engineering* 23:208-215.
- Lauffenburger, D.A., J.J. Linderman. 1993. *Receptors: models for binding, trafficking, and signalling*. Oxford University Press, New York
- Lee, J.R., S. Urban, C.F. Garvey, M. Freeman. 2001. Regulated intracellular ligand transport and proteolysis regulate egf receptor activation in Drosophila. *Cell* 107:161-71.
- Ma, Z., D. Webb, M. Jo, S. Gonias. 2001. Endogenously produced urokinase-type plasminogen activator is a major determinant of the basal level of activated

- ERK/MAP kinase and prevents apoptosis in MDA-MB-231 breast cancer cells. *J Cell Sci* 114:3387-96.
- Mandell, J.W., N.C. Gocan, S.R. Vandenberg. 2001. Mechanical trauma induces rapid astroglial activation of ERK/MAP kinase: Evidence for a paracrine signal. *Glia* 34:283-95.
- Mantrova, E., T. Hsu. 1998. Down-regulation of transcription factor CF2 by Drosophila Ras/MAP kinase signaling in oogenesis: cytoplasmic retention and degradation. *Genes and Development* 12:1166-75.
- Merlos-Suarez, A., S. Ruiz-Paz, J. Baselga, J. Arribas. 2001. Metalloprotease-dependent protransforming growth factor- α ectodomain shedding in the absence of tumor necrosis factor- α -converting enzyme. *J Biol Chem* 276:48510-7.
- Mikhailov, A.S. 1994. Foundations of synergetics. Springer, Berlin, New York
- Moghal, M., P.W. Sternberg. 1999. Multiple positive and negative regulators of signaling by the EGF-receptor. *Current Opinion in Cell Biology* 11:190-6.
- Montero, J., L. Yuste, E. Diaz-Rodriguez, A. Espasis-Ogando, A. Pandiella. 2000. Differential Shedding of Transmembrane Neuregulin Isoforms by Tumor Necrosis-factor- α -converting enzyme. *Molecular and Cellular Neuroscience* 16:631-648.
- Montero, J.C., L. Yuste, E. Diaz-Rodriguez, A. Esparis-Ogando, A. Pandiella. 2002. Mitogen-activated protein kinase-dependent and -independent routes control shedding of transmembrane growth factors through multiple secretases. *Biochem J* 363:211-21.
- Muller, S.C., T. Mair, O. Steinbock. 1998. Traveling waves in yeast extract and in cultures of Dictyostelium discoideum. *Biophys Chem* 72:37-47.
- Murphy, L., M. Cluck, S. Lovas, F. Otvos, R. Murphy, A. Schally, J. Permert, J. Larsson, J. Knezetic, T. Adrian. 2001. Pancreatic cancer cells require and EGF receptor-mediated autocrine pathway for proliferation under serum-free conditions. *British Journal of Cancer* 84:926-35.
- Ni, C.Y., M.P. Murphy, T.E. Golde, G. Carpenter. 2001. γ -Secretase cleavage and nuclear localization of ErbB-4 receptor tyrosine kinase. *Science* 294:2179-81.
- Palsson, E., K.J. Lee, R.E. Golstein, J. Franke, R.H. Kessin, E. Cox. 1997. Selection for spiral waves in the social amoebae Dictyostelium. *Proc Natl Acad Sci* 94:13719-23.
- Peri, F., C. Bokel, S. Roth. 1999. Local Gurken signaling and dynamic MAPK activation during Drosophila oogenesis. *Mechanisms of Development* 81:75-88.
- Peschon, J.J., J.L. Slack, P. Reddy, K.L. Stocking, S.W. Sunnarborg, D.C. Lee, W.E. Russell, B. Castner, R.S. Johnson, J.N. Fitzner, R. Boyce, N. Nelson, C.J. Kozlosky, M.F. Wolfson, C.T. Rauch, D.P. Cerretti, R.J. Paxton, C.J. March, R.A. Black. 1998. An essential role for ectodomain shedding in mamalian development. *Science* 282:1281-4.
- Pierce, K.L., A. Tohgo, S. Ahn, M.E. Field, L.M. Luttrell, R.J. Lefkowitz. 2001. Epidermal growth factor (EGF) receptor-dependent ERK activation by G protein-coupled receptors: a co-culture system for identifying intermediates upstream and downstream of heparin-binding EGF shedding. *J Biol Chem* 276:23155-60.

- Sapir, A., R. Schweitzer, B.Z. Shilo. 1998. Sequential activation of the EGF receptor pathway during *Drosophila* oogenesis establishes the dorsoventral axis. *Development* 125:191-200.
- Scemes, E., S.O. Suadicani, D.C. Spray. 2000. Intercellular communication in spinal cord astrocytes: fine tuning between gap junctions and P2 nucleotide receptors in calcium wave propagation. *J Neurosci* 20:1435-45.
- Schlessinger, J. 2000. Cell signaling by receptor tyrosine kinases. *Cell* 103:211-25.
- Schoeberl, B., C. Eichler-Jonsson, E.D. Gilles, G. Muller. 2002. Computational modeling of the dynamics of the MAP kinase cascade activated by surface and internalized EGF receptors. *Nat Biotechnol* 20:370-5.
- Schuster, S., M. Marhl, T. Hofer. 2002. Modelling of simple and complex calcium oscillations. From single-cell responses to intercellular signalling. *Eur J Biochem* 269:1333-55.
- Shiga, H., T. Tojima, E. Ito. 2001. Ca²⁺ signaling regulated by an ATP-dependent autocrine mechanism in astrocytes. *Neuroreport* 12:2619-22.
- Shvartsman, S.Y., M.P. Hagan, A. Yacoub, P. Dent, H.S. Wiley, D.A. Lauffenburger. 2002. Autocrine loops with positive feedback enable context-dependent cell signaling. *Am J Physiol Cell Physiol* 282:C545-C549.
- Shvartsman, S.Y., H.S. Wiley, W.M. Deen, D.A. Lauffenburger. 2001. Spatial range of autocrine signaling: modeling and computational analysis. *Biophysical Journal* 81:1854-67.
- Slepchenko, B.M., J.C. Schaff, J.H. Carson, L.M. Loew. 2002. Computational cell biology: spatiotemporal simulation of cellular events. *Annu Rev Biophys Biomol Struct* 31:423-41.
- Sneyd, J., M. Wilkins, A. Strahonja, M.J. Sanderson. 1998. Calcium waves and oscillations driven by an intercellular gradient of inositol (1,4,5)-trisphosphate. *Biophys Chem* 72:101-9.
- Sommeijer, B.P., L.F. Shampine, J.G. Verwer. 1998. RKC: An explicit solver for parabolic PDEs. *J Comput Appl Math* 88:315-326.
- Spradling, A.C. 1993. Developmental Genetics of oogenesis. The development of *Drosophila Melanogaster*. Plainview: Cold Spring Harbor Laboratory Press. p 1-70.
- Sturtevant, M.A., J.W. O'Neill, E. Bier. 1994. Down-regulation of *Drosophila* Egf-r mRNA levels following hyperactivated receptor signaling. *Development* 120:2593-600.
- Sunnarborg, S.W., C.L. Hinkle, M. Stevenson, W.E. Russell, C.S. Raska, J.J. Peschon, B.J. Castner, M.J. Gerhart, R.J. Paxton, R.A. Black, D. Lee. 2002. Tumor necrosis factor-alpha converting enzyme (TACE) regulates epidermal growth factor receptor ligand availability. *J Biol Chem* 277:12838-45.
- Tang, Y., H.G. Othmer. 1995. Excitation, oscillations and wave propagation in a G-protein-based model of signal transduction in *Dictyostelium discoideum*. *Philos Trans R Soc Lond B Biol Sci* 349:179-95.
- Tang, Y., J.L. Stephenson, H.G. Othmer. 1996. Simplification and analysis of models of calcium dynamics based on IP₃-sensitive calcium channel kinetics. *Biophys J* 70:246-63.

- Umata, T., M. Hirata, T. Takahashi, F. Ryu, S. Shida, Y. Takahashi, M. Tsuneoka, Y. Miura, M. Masuda, Y. Horiguchi, E. Mekada. 2001. A dual signaling cascade that regulates the ectodomain shedding of heparin-binding epidermal growth factor-like growth factor. *J Biol Chem* 276:30475-30482.
- Wasserman, J.D., M. Freeman. 1998. An autoregulatory cascade of EGF receptor signaling patterns the Drosophila egg. *Cell* 95:355-364.
- Wiley, H., P. Burke. 2001. Regulation of receptor tyrosine kinase signaling by endocytic trafficking. *Traffic* 2:13-18.
- Wiley, H.S., J.J. Herbst, B. Walsh, D.A. Lauffenburger, M.G. Rosenfeld, G. Gill. 1991. The role of tyrosine kinase activity in endocytosis, compartmentation, and downregulation of the epidermal growth factor receptor. *J Biol Chem* 266:11083-11094.
- Yan, Y., K. Shirakabe, Z. Werb. 2002. The metalloprotease Kuzbanian (ADAM10) mediates the transactivation of EGF receptor by G protein-coupled receptors. *J Cell Biol* 158:221-6.
- Zhang, Z., P. Oliver, S.R. Lancaster, P.O. Schwarzenberger, M.S. Joshi, J. Cork, J.K. Kolls. 2000. Reactive oxygen species mediate tumor necrosis factor alpha-converting, enzyme-dependent ectodomain shedding induced by phorbol myristate acetate. *FASEB Journal*:303-305.

TABLE 1 MODEL PARAMETERS

Parameter	Description	Range
D	ligand diffusivity	$1 \times 10^{-12} - 1 \times 10^{-10} \text{ m}^2 \text{ s}^{-1}$
h	height of the extracellular medium	$10 \text{ } \mu\text{m} - 1000 \text{ } \mu\text{m}$
k_{ec}	ligand-induced internalization rate constant	$0.01 - 0.3 \text{ min}^{-1}$
k_{er}	constitutive internalization rate constant	$0.01 - 0.1 \text{ min}^{-1}$
k_{on}	receptor/ligand association constant	$1 \times 10^3 - 1 \times 10^6 \text{ m}^3 \text{ mol}^{-1} \text{ min}^{-1}$
k_p	protease degradation rate constant	0.01 min^{-1}
$K_D = k_{off}/k_{on}$	ligand/receptor-complex equilibrium constant	$1 \times 10^{-7} - 1 \times 10^{-5} \text{ mol m}^{-3}$
$R_0 = Q_r/k_{er}$	number of receptors per cell surface in absence of a ligand	$1 \times 10^3 - 1 \times 10^6$ receptors/cell surface area

FIGURE CAPTIONS:

FIGURE 1 Positive feedback in autocrine systems. (A) The feedback is mediated by the activation of the ligand-releasing enzyme. (B) Positive feedback relying on transcription. Intracellular signaling activated by autocrine ligands induces and maintains the transcription of the ligand-releasing enzyme. (C) The geometry of cell communication in the model of an autocrine relay. Ligand is diffusing in extracellular medium above the cellular layer. (D) Receptor-mediated processes in the model: ligand release, extracellular transport, reversible binding, and endocytosis. D – ligand diffusivity, k_{on} – ligand-receptor association constant, k_{off} – complex dissociation constant, k_{ec} – ligand-induced internalization rate constant.

FIGURE 2 (A) Graphical solution of Equation 14, where $\sigma(c)$ is chosen to be a Hill function $\sigma(c) = c^n / (k^n + c^n)$. (B) The case of the Heaviside nonlinearity: $\sigma(c) = H(c - c_0)$. No ligand is released in the “off” steady state. Autocrine loop is activated in the “on” steady state.

FIGURE 3 A traveling front in the ligand-limited regime with fast binding and sharp nonlinearity of protease activation (see Appendix A). (A) and (B) present the profiles of the extracellular ligand and ligand-releasing protease, respectively. The arrows denote the direction of wave’s motion. The value of the dimensionless velocity is $v = 1.967$, the threshold in the Heaviside function $c_0 = 0.25$. Other dimensionless model parameters are $\alpha = 55.36$, $\beta = 0.5$, $\tau_s = 5.439 \times 10^{-4}$ (based on $k_{on} = 1 \times 10^5 \text{ m}^3 \text{ mol}^{-1} \text{ min}^{-1}$, R_0 is based on 5×10^4 receptors/cell surface area ($25 \text{ } \mu\text{m}^2$), $k_{ec} = 0.1 \text{ min}^{-1}$, $k_{off} = 0.1 \text{ min}^{-1}$, $D = 1 \times 10^{-10} \text{ m}^2 \text{ s}^{-1}$, $k_p = 0.01 \text{ min}^{-1}$, $h = 1 \times 10^3 \text{ } \mu\text{m}$).

FIGURE 4. Dependence of the dimensional front speed on the kinetic and transport parameters in the ligand-limited regime with fast binding and sharp nonlinearity of protease activation (see Appendix A). (A) Dependence on the rate of forward binding on

the forward-binding rate constant, $k_{on}R_0$, ligand-induced internalization rate constant k_{ec} and complex dissociation constant k_{off} . The dark red area corresponds to the maximal value of the velocity ($v \approx 4 \times 10^{-2} \mu\text{ms}^{-1}$). Conversely, the dark blue area denotes the minimal value of the velocity ($v \approx 4 \times 10^{-4} \mu\text{ms}^{-1}$). The threshold in the Heaviside function $c_0 = 0.25$. Other model parameters are $h = 1 \times 10^3 \mu\text{m}$, $D = 1 \times 10^{-10} \text{m}^2\text{s}^{-1}$, $k_p = 0.01 \text{min}^{-1}$. (B) A one dimensional cut ($k_{ec}/(k_{ec} + k_{off}) = 0.5$) through the two-parameter plot in (A). The arrows indicate that increasing the ratio $k_{ec}/(k_{ec} + k_{off})$ shifts the velocity maximum to a lower value of $k_{on}R_0$.

FIGURE 5 Dependence of the wave propagation velocity on the ratio of the geometric length scale h and the dynamic length scale L_x in the ligand-limited regime with fast binding and sharp nonlinearity of protease activation (see Appendix A). (A) Dependence of the dimensionless velocity on the ratio h/L_x computed for several thresholds c_0 in the Heaviside function. The propagation velocity increases with the ratio until $\log_{10}(h/L_x) \approx 1$. Above this value, the velocity does not depend on this geometric parameter. The parameters are $\beta = 0.5$, $\tau_s = 5.439 \times 10^{-4}$ (based on $k_{on} = 1 \times 10^5 \text{m}^3\text{mol}^{-1}\text{min}^{-1}$, R_0 is based on 5×10^4 receptors/cell surface area ($25 \mu\text{m}^2$), $k_{ec} = 0.1 \text{min}^{-1}$, $k_{off} = 0.1 \text{min}^{-1}$, $D = 1 \times 10^{-10} \text{m}^2\text{s}^{-1}$, $k_p = 0.01 \text{min}^{-1}$). (B). Colormaps of the distributions $s(\zeta, \eta)$ of the ligand in a traveling wave in both horizontal and vertical directions, with $c_0 = 0.25$. The spatial distributions of the ligand correspond to the filled circles in (A). The profiles were computed for $\log_{10}(h/L_x) = -1, 0, 1, 2$. The dark red/dark blue regions correspond to the “on”/“off” steady states ($s = 1, s=0$), respectively.

FIGURE 6. Numerical analysis of the full model. (A) and (B) Ligand and protease distributions computed across the front. The ligand release function is modeled by a Hill function $\sigma(c) = c^n / (k^n + c^n)$, with $k = 0.25$ and $n = 5$. Other parameters are $\alpha = 1$, $\beta = 0.5$, $\gamma = 0.2$, $\tau_c = 0.1$, $\tau_s = 3.334$, $\tau_r = 2$. (based on $k_{on} = 1.807 \times 10^3 \text{m}^3\text{mol}^{-1}\text{min}^{-1}$, $R_0 = Q_r/k_{er}$ is based on 5×10^4 receptors/cell surface area ($Q_r = 500$ receptors/cell surface/min,

$k_{er} = 0.01 \text{ min}^{-1}$, cell surface area $25 \mu\text{m}^2$), $k_{ec} = 0.1 \text{ min}^{-1}$, $k_{off} = 0.1 \text{ min}^{-1}$, $D = 1 \times 10^{-10} \text{ m}^2 \text{ s}^{-1}$, $k_p = 0.02 \text{ min}^{-1}$, $h = 1 \times 10^3 \mu\text{m}$, $Q_l = g_r g_p / k_p = 50$ ligand molecules/cell surface/min). (C) The wave velocity was computed from the linear part of the dependence of the front position on time. (D) Dependence of the wave propagation velocity on the ligand-receptor affinity $k_{on}R_0$. The points are the results of the numerical analysis; the curve is drawn to guide the eye.

FIGURE 7. Interaction of fronts with heterogeneities in the cellular layer. (A) The heterogeneities can both accelerate and slow down the fronts. (B,C) – the location of the front as a function of time in an intact (solid line) and damaged layer (broken line). (B) The case of low binding rate, $k_{on}R_0 = 0.1 \mu\text{ms}^{-1}$ (based on $k_{on} = 1.807 \times 10^3 \text{ m}^3 \text{ mol}^{-1} \text{ min}^{-1}$). The extent of the damaged tissue is $\Delta x / L_x = 2.5$. The values of the parameters of the Hill nonlinearity and the other model parameters are the same as in Figure 6A,B. (C) The case of high ligand-receptor affinity $k_{on}R_0 = 10 \mu\text{ms}^{-1}$ (based on $k_{on} = 1.807 \times 10^5 \text{ m}^3 \text{ mol}^{-1} \text{ min}^{-1}$). The extent of the damaged tissue is $\Delta x / L_x = 10$. Other parameters as in Figure 6A,B.

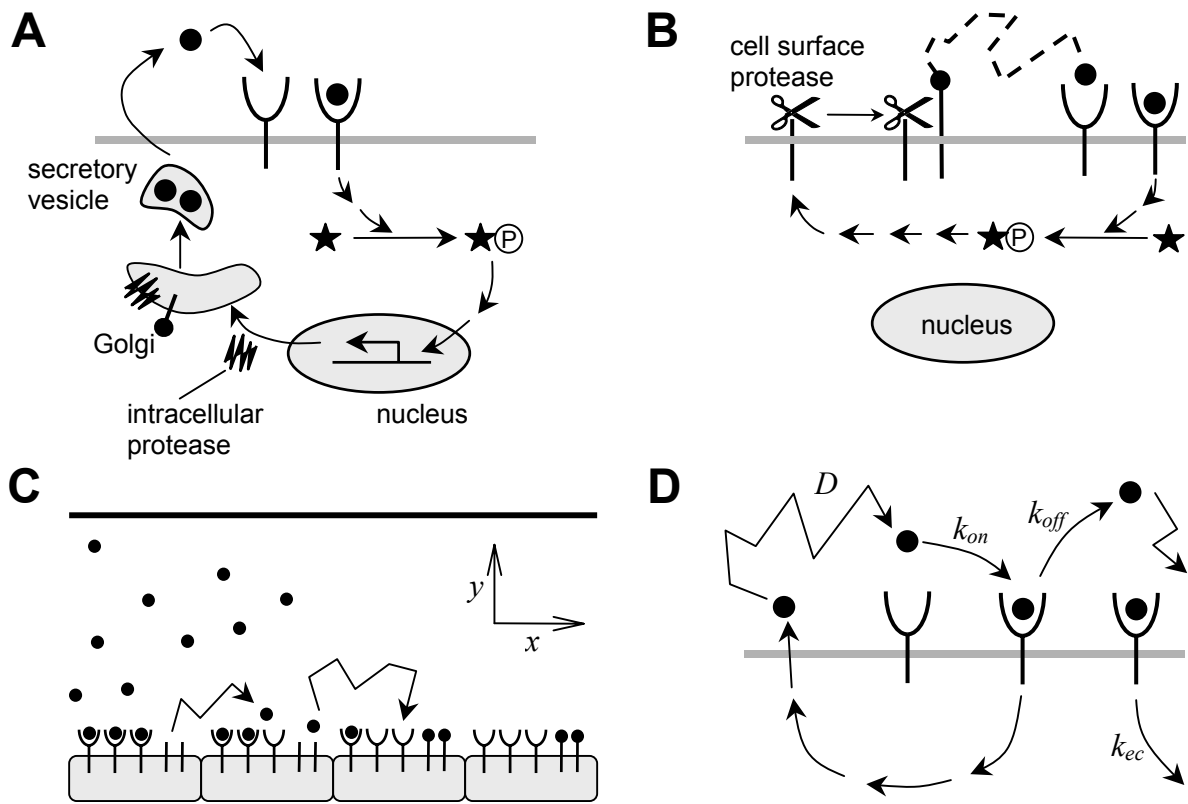


FIGURE 1

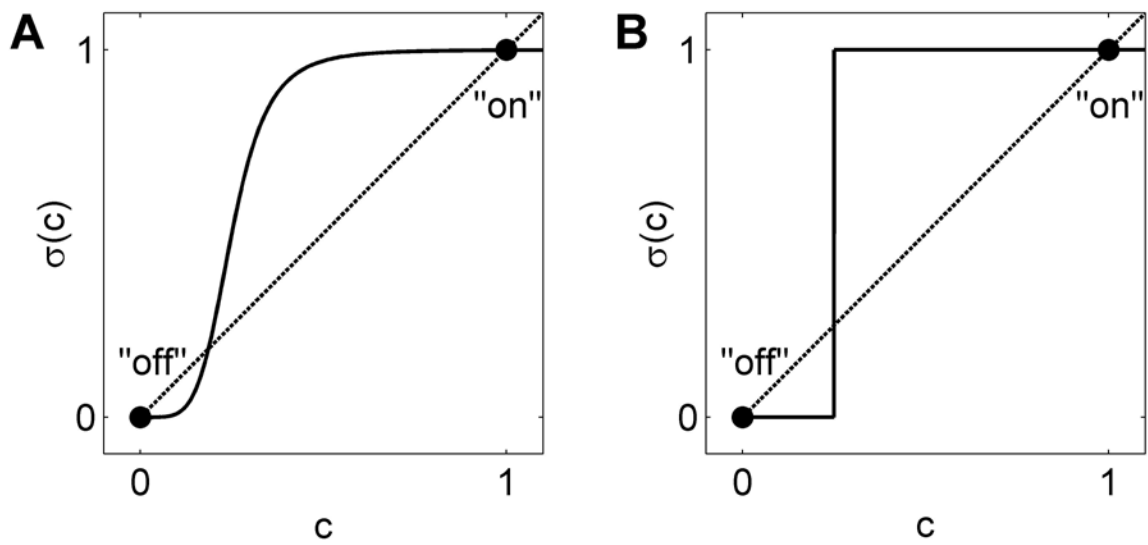


FIGURE 2

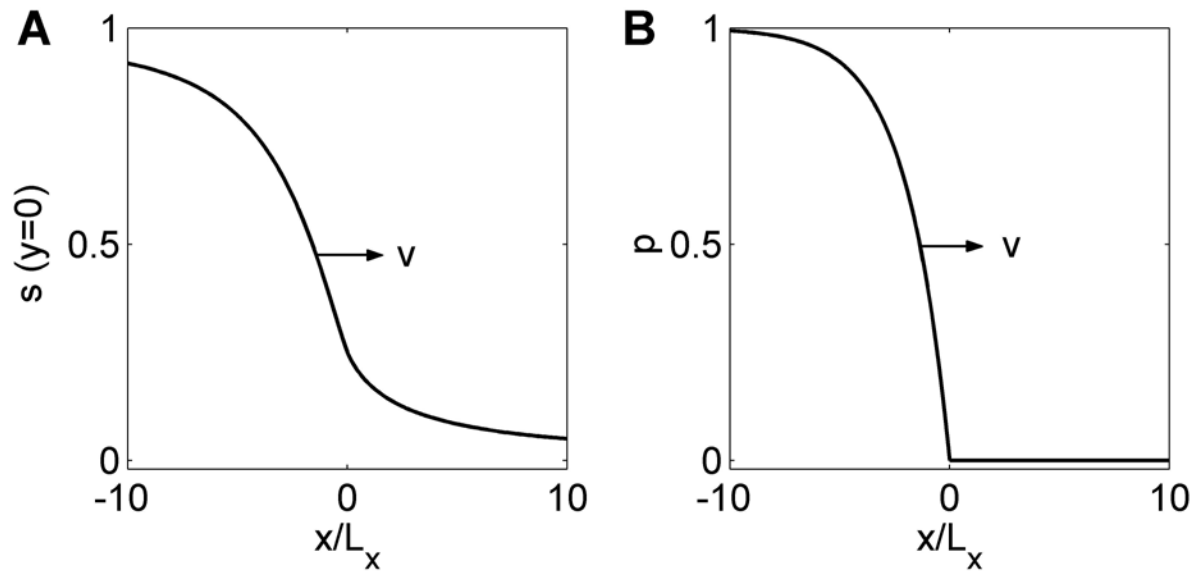


FIGURE 3

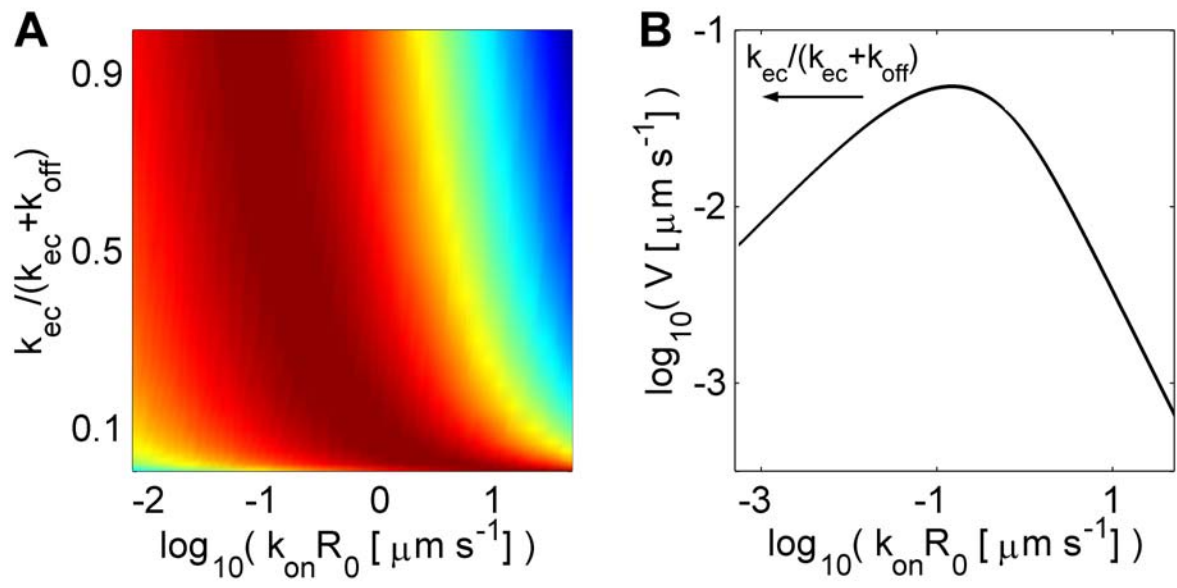


FIGURE 4

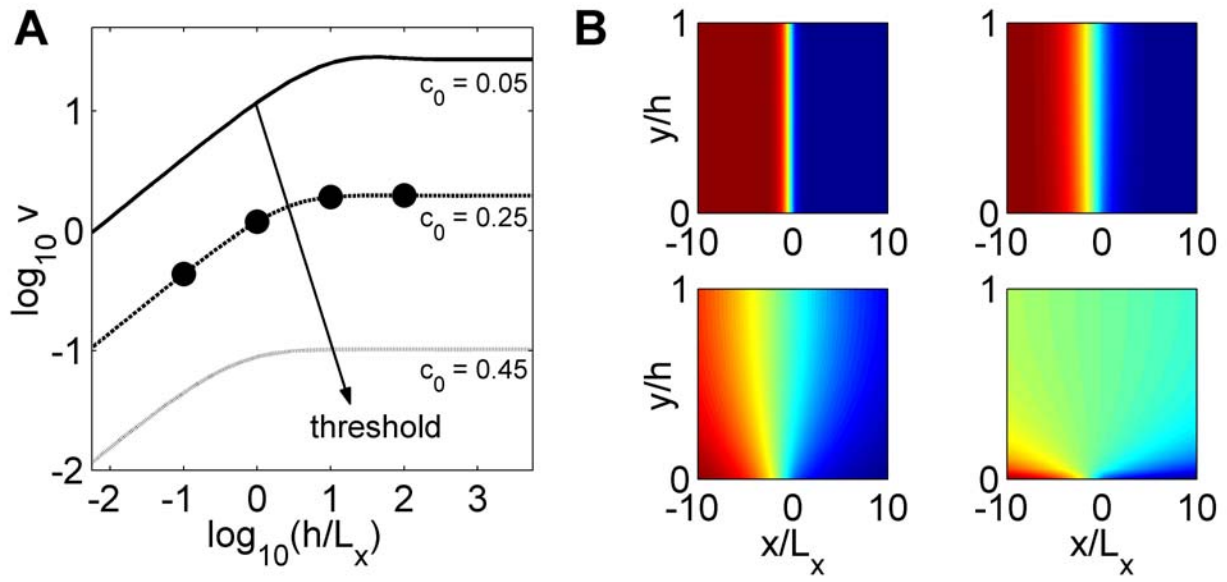


FIGURE 5

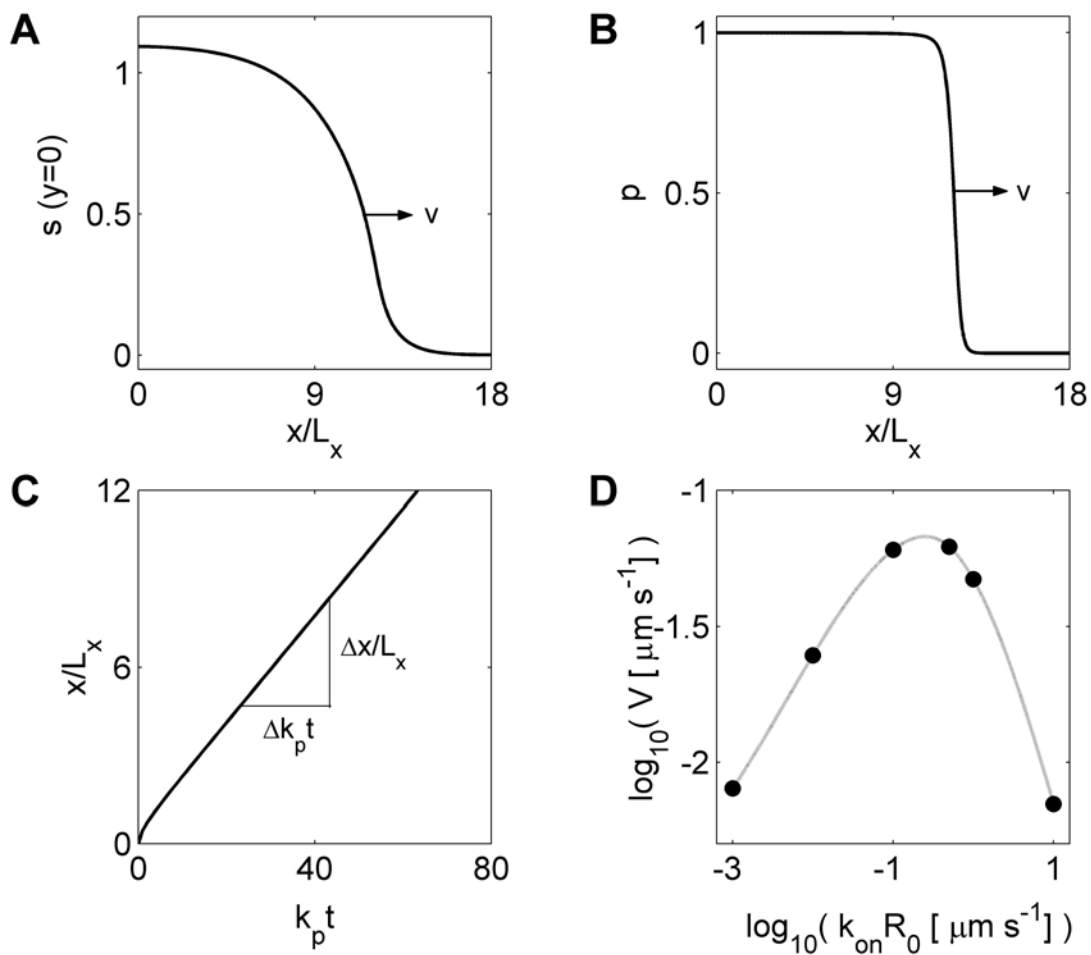


FIGURE 6

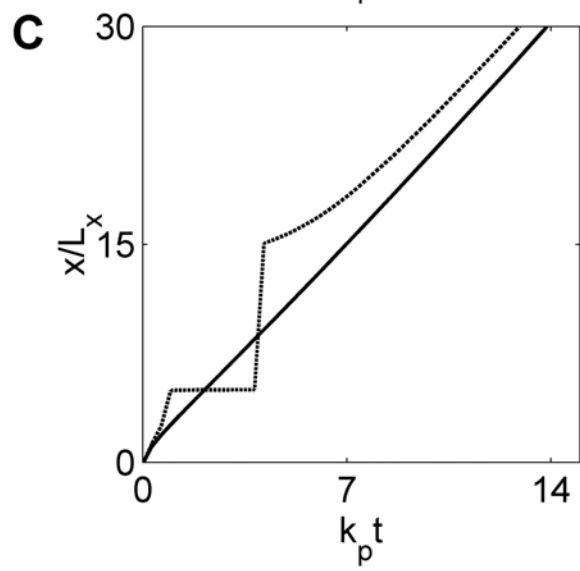
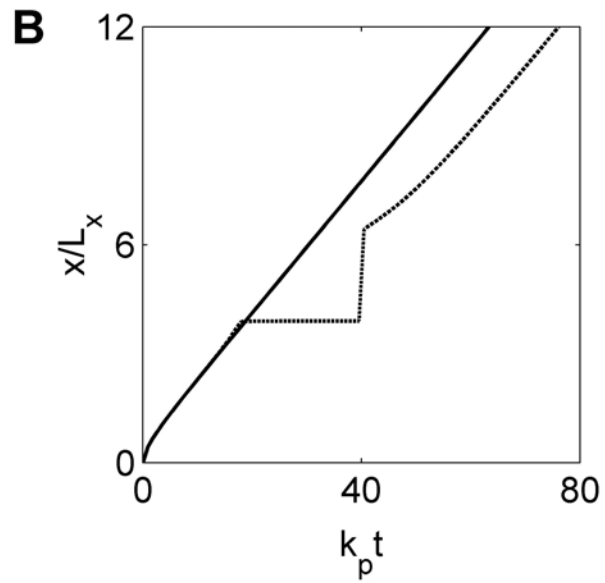
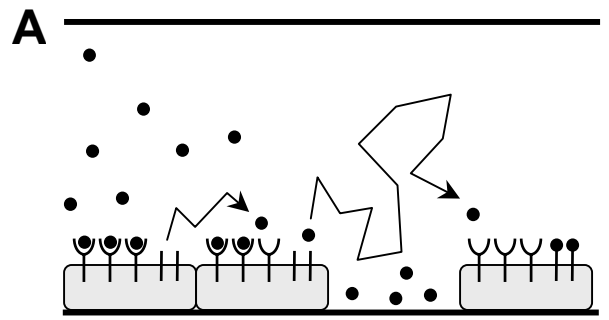


FIGURE 7